Cai et al.
Protection and Control of Modern Power Systems (2023) 8:34
https://doi.org/10.1186/s41601-023-00307-9

Protection and Control of Modern Power Systems

ORIGINAL RESEARCH Open Access

Hierarchical under frequency load shedding scheme for inter-connected power systems

Guowei Cai[1], Shuyu Zhou[1], Cheng Liu[1*], Yuchi Zhang[1], Shujia Guo[1] and Zhichong Cao[1]

Abstract

Severe disturbances in a power network can cause the system frequency to exceed the safe operating range. As the last defensive line for system emergency control, under frequency load shedding (UFLS) is an important method for preventing a wide range of frequency excursions. This paper proposes a hierarchical UFLS scheme of "centralized real-time decision-making and decentralized real-time control" for inter-connected systems. The centralized decision-layer of the scheme takes into account the importance of the load based on the equivalent transformation of kinetic energy (KE) and potential energy (PE) in the transient energy function (TEF), while the load PE is used to determine the load shedding amount (LSA) allocation in different loads after faults in real-time. At the same time, the influence of inertia loss is considered in the calculation of unbalanced power, and the decentralized control center is used to implement the one-stage UFLS process to compensate for the unbalanced power. Simulations are carried out on the modified New England 10-generator 39-bus system and 197-bus system in China to verify the performance of the proposed scheme. The results show that, compared with other LSA allocation indicators, the proposed allocation indicators can achieve better f_{nadir} and t_d. At the same time, compared with other multi-stage UFLS schemes, the proposed scheme can obtain the maximum f_{nadir} with a smaller LSA in scenarios with high renewable energy sources (RES) penetration.

Keywords Hierarchical under frequency load shedding, Centralized real-time decision-making and decentralized real-time control, Transient energy function, Kinetic energy, Potential energy

1 Introduction

1.1 Background and motivation

When a power system suffers from extreme faults such as power transmission line disconnection, loss of large power generation, etc., the system will have large unbalanced power. The large frequency deviation caused by the unbalanced power can damage power generation equipment, and even, in severe cases, cause the system to collapse [1]. Thus, emergency control measures are needed to maintain the balance between generation and demand within the system. As the third line of defense, under frequency load shedding (UFLS) is an important method for restoring frequency stability and reducing system unbalanced power [2, 3]. With the rapid development of the modern power system, the penetration of renewable energy sources (RES) in the system is increasing. As most RES are connected to the system via power electronic interfaces, they provide little or no inertia to the system [4]. The decrease of system inertia will lead to a higher rate of change of frequency, which may render existing UFLS schemes ineffective, causing the frequency to be outside the safe range. Therefore, it is necessary to design an appropriate UFLS scheme in the current power system.

*Correspondence:
Cheng Liu
05dylc@163.com
[1] School of Electrical Engineering, Northeast Electrical Power University, Jilin 132012, China

1.2 Literature review

The key to better performance of a UFLS scheme is accurate evaluation and allocation of unbalanced power in real-time after faults [5–8]. The unbalanced power determines the amount of load that needs to be removed, and the evaluation results that are too high or too low cannot fully reflect the effect of the UFLS scheme. Therefore, in [8], the unbalanced power evaluation method based on the rate of change of COI frequency is studied. However, because of the voltage characteristics of the load, the unbalanced power evaluation results in [8] are biased. In [9], load power deviation is introduced to correct the unbalanced power in [8]. To solve the problems of communication delay and excessive data processing caused by COI frequency calculation, an evaluation method for the rate of change of COI frequency based on local measurement is developed in [10] using inflection point detection technology, and the change of system inertia is also considered.

As for the allocation of load shedding amount (LSA), it is verified in [11] by simulation that the performance of load shedding (LS) with different priorities is different for the UFLS scheme. In [12], when the LSA is determined, particle swarm optimization is used to solve the optimal LS combination. However, the above method requires a large amount of calculation so is mostly used for off-line strategy formulation, as it is difficult for it to be embedded in UFLS relays with a strict requirement on calculation speed. In [13], the influence of unbalanced power on load voltage is considered, and the sensitivity of load reactive power to voltage is used for LSA allocation. In [14], the rate of load voltage drop is used for LSA allocation, while in [15], the voltage amplitude is considered on the basis of [14]. In [16], a voltage stability index (VSI) based on the Thevenin equivalent model of the load bus is proposed to quickly search for suitable locations for LS, whereas in [17], the influence of a photovoltaic power station on the Thevenin equivalent model of load nodes is considered on the basis of [16]. The above LSA allocation is analyzed from the perspective of voltage stability, without establishing a relationship with frequency stability. In [18], steady-state load power and frequency deviation are used for LSA allocation. Among them, the load bus with larger initial load power and frequency deviation will share a larger LSA. In [19], a simple and efficient method is proposed to calculate the sensitivity of system frequency to load power variation, and the load which has greater influence on the system frequency is identified. However, this method needs accurate generator parameter information, which is difficult to obtain directly from measurement data. As the analysis of the above indicators does not establish a detailed mechanism model to yield the relationship between each load and the system frequency, so it is impossible to reveal the degree of influence of each load on the system frequency stability. Therefore, the construction of a multi-machine system model for frequency stability analysis is crucial.

1.3 Contribution and organization

The transient energy function (TEF) of a multi-machine system is a good model for analyzing system stability. It comes from Lyapunov stability theory and follows the basic law of energy conservation [4, 20, 21]. In the dynamic process after the system is disturbed, the energy will be transformed and interact with each other in the system in the form of kinetic energy (KE) and potential energy (PE) [20], while the total amount of energy remains unchanged. Therefore, the conversion relationship between the rotor KE and the system PE (the PE of load, line, etc.) can be established through the TEF, where the rotor KE can reflect the system frequency change [20]. Then, the factors of load that affect the KE can be analyzed, and the influence of different loads on the system frequency can be analyzed from the perspective of energy.

In this paper, the TEF in [21] is extended by using Telleggen's theorem, so that it can consider the grid connection of RES, and can be applied to the case of system unbalanced power disturbance. The reference point in the TEF is discussed to make it more suitable for the real fault trajectory change of the system. Then, a hierarchical UFLS scheme based on PUMs is proposed. The key in this scheme is the calculation and allocation of LSA. Based on the principle of KE and PE transformation in TEF, the PE of load is used to consider the allocation of LSA, while the LSA calculation takes into account the impact of the loss of the generation. The main contributions of this paper are as follows:

1. For the imbalance power disturbance in the system, a multi-machine system TEF model conforming to the actual fault trajectory of the system is constructed based on [21]. This takes into account a highly concentrated RES scenario.
2. Based on the principle of KE and PE transformation in the TEF, a LSA allocation indicator is proposed. On this basis, a one-stage hierarchical UFLS scheme using measurement data is proposed, and the inertia change of the system is considered.
3. Comparison with other LSA allocation indicators verifies the advantages of those proposed. A comparison with the multi-stage UFLS scheme verifies that the one-stage UFLS scheme is more appropriate in the "centralized real-time decision-making and decentralized real-time control" framework.

The remainder of this paper is organized as follows. In Sect. 2, the TEF of the multi-machine system is constructed, whereas in Sect. 3, the proposed UFLS scheme based on load PE is described. Simulations are presented in Sect. 4, and conclusions are presented in Sect. 5

2 Theoretical basis for the proposed scheme

2.1 Transient energy function construction

A TEF based on the structure-preserving model is used as an analysis method for the traditional power angle stability problem [4, 20, 21]. A simple system TEF based on the second-order equation of rotor motion is constructed in [21], though it only contains the KE of the generator and the PE of the lines. This section extends the TEF in [21], considering the governor system, load and RES (includes wind power, photovoltaics, and DC fed from an external grid). Among them, RES has no inertia and fast frequency response capability, while the line losses in the system are ignored.

For an n-machine h-node system, the total number of nodes in the system is $n+h$, and the swing equation of the generator i can be expressed as:

$$\frac{d\delta_i}{dt} = \Delta f_i \tag{1a}$$

$$M_{gi}\frac{d\Delta f_i}{dt} = P_{mi} - P_{ei} \quad i = 1, 2, \cdots n \tag{1b}$$

where δ_i is the power angle, Δf_i is the frequency deviation, P_{ei} and P_{mi} are the respective electromagnetic and mechanical power, and M_{gi} is the mechanical time constant of the generator.

The TEF of the overall system can be represented as [21]:

$$\begin{aligned} V &= V_{KE} + V_{PE} \\ &= \sum_{i=1}^{n}\frac{1}{2}M_{gi}\Delta f_i^2 - \sum_{i=1}^{n}\int_{t^{ss}}^{t}(P_{mi} - P_{ei})\Delta f_i dt \quad i = 1, 2, \ldots n \end{aligned} \tag{2}$$

where V_{KE} is the total KE of the system.

According to the balance relationship of active power flow, the following balance equation exists for any node i in the network [22]:

$$P_{ei} + P_{wi} - P_{li} = \sum_{j=1}^{n+h} U_i U_j \sin\theta_{ij}/X_{ij} \quad i = 1, \ldots n+h \tag{3}$$

where P_{wi} and P_{li} are the post-fault power of RES and load, respectively.

Multiplying both sides of (3) by Δf_i, and given $X_{ij} = X_{ji}$ and $\sin\theta_{ij} = -\sin\theta_{ji}$, the $n+h$ node equations in (3) are summed as [20]:

$$\begin{aligned} \sum_{i=1}^{n+h}P_{ei}\Delta f_i + \sum_{i=1}^{n+h}P_{wi}\Delta f_i - \sum_{i=1}^{n+h}P_{li}\Delta f_i &= \sum_{i=1}^{n+h}\sum_{j=1}^{n+h}U_iU_j\sin\theta_{ij}/X_{ij}\Delta f_i \\ &= \sum_{i=1}^{n+h-1}\sum_{j=i+1}^{n+h}U_iU_j\sin\theta_{ij}/X_{ij}f_{ij} \\ &= \sum_{b=1}^{k}P_b f_b \end{aligned} \tag{4}$$

where $P_b = U_iU_j\sin\theta_{ij}/X_{ij}$, $f_b = f_{ij}$, and k is the total number of lines in system.

For a lossless power network, the active power of each line satisfies Kirchhoff's current theorem, and the frequency of each node satisfies Kirchhoff's voltage theorem. Considering that the system has the same topology in transient and steady state after fault, the equivalent network diagram of the system is shown in Fig. 1. According to Tellegen's second theorem [23], there is:

$$\sum_{i=1}^{n+h}P_{mi}^{ss}\Delta f_i + \sum_{i=1}^{n+h}P_{wi}^{ss}\Delta f_i - \sum_{i=1}^{n+h}P_{li}^{ss}\Delta f_i = \sum_{b=1}^{k}P_b^{ss}f_b \tag{5}$$

where $P_{mi}^{ss} = P_{ei}^{ss}$,$P_{ei}^{ss}$,$P_{mi}^{ss}$,$P_{wi}^{ss}$,$P_{li}^{ss}$ and P_b^{ss} are the electromagnetic power, mechanical power, RES power, load power and line power in post-fault steady state point.

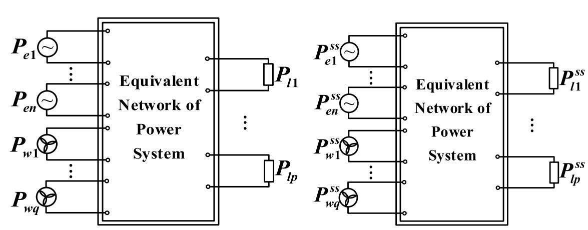

Fig. 1 System transient equivalent network diagram and its post-fault steady state adjoint network

Subtracting (4) and (5), and bringing the results into (2), the TEF of the whole system can be obtained, as:

$$\begin{aligned} V &= V_{KE} + V_{PE} \\ &= V_{KE} + V_{PE,m} + V_{PE,w} + V_{PE,l} + V_{PE,b} \\ &= \sum_{i=1}^{n} \frac{1}{2} M_{gi} \Delta f_{gi}^2 - \sum_{i=1}^{n} \int_{t^{ss}}^{t} (P_{mi} - P_{mi}^{ss}) \Delta f_{gi} dt - \sum_{i=1}^{q} \int_{t^{ss}}^{t} (P_{wi} - P_{wi}^{ss}) \Delta f_{wi} dt \\ &+ \sum_{i=1}^{p} \int_{t^{ss}}^{t} (P_{li} - P_{li}^{ss}) \Delta f_{li} dt + \sum_{b=1}^{k} \int_{t^{ss}}^{t} (P_b - P_b^{ss}) f_b \Delta f_b dt \end{aligned} \tag{6}$$

Where V, $V_{PE,m}$, $V_{PE,w}$, $V_{PE,l}$ and $V_{PE,b}$ are the TEF, total PE of generator, RES, load and line of the system based on the post-fault steady-state point, respectively.

2.2 Discussion of steady-state reference points for transient energy function

The construction of the above TEF is based on the post-fault steady-state point as the steady-state reference point. This is to meet the positive definiteness requirement of the Lyapunov direct method for the function $\boldsymbol{V}$. This makes the TEF puzzling in the physical mechanism. In order to select the post-fault steady-state point as the steady-state reference point, a virtual steady-state time t_{ss} has to be defined. The dynamic mechanism of the system transient process is the energy conservation and conversion process, and the energy accumulation process starts from the pre-fault steady-state point, rather than the post-fault steady-state point. The PE term of the TEF is related to the trajectory of the system, and it is difficult to imagine what the trajectory of the system would look like from a post-fault steady-state point. Therefore, from the dynamic point of view, the selection of the post-fault steady-state point lacks basis.

To solve the above problems, this chapter will discuss the selection of the reference point of the TEF. Here, the PE of (2) is rewritten as:

$$\begin{aligned} V_{PE} &= \sum_{i=1}^{n} \int_{t^{ss}}^{t} (P_{ei} - P_{mi}) \Delta f_i dt \\ &= \sum_{i=1}^{n} \left(\int_{t_0}^{t} (P_{ei} - P_{mi}) \Delta f_i dt + \int_{t^{ss}}^{t_0} (P_{ei} - P_{mi}) \Delta f_i dt \right) \\ &= \hat{V}_{PE} + C \end{aligned} \tag{7}$$

where t_0 is the time corresponding to the pre-fault steady-state point of the system. $\hat{V}_{PE} = \sum_{i=1}^{n} (\int_{t_0}^{t} (P_{ei} - P_{mi}) \Delta f_i dt$ is the PE of the system based on the pre-fault steady-state point, and $\int_{t^{ss}}^{t_0} (P_{ei} - P_{mi}) \Delta f_i dt$ can be considered as a constant C.

Through the analysis of (7), it can be seen that the difference of the steady-state reference points will affect the magnitude of the system PE, but it does not affect its changing trend. In any time period [t_a, t_b] after the fault, there exists the following relationship:

$$V_{PE}\big|_{t_a}^{t_b} = \hat{V}_{PE}\Big|_{t_a}^{t_b} \tag{8}$$

Equation (8) shows that the PE increment of the system at any two moments is not linked to the selection of the steady-state reference point.

Based on the above analysis, the pre-fault steady-state point is selected as the steady-state reference point, which is consistent with the real dynamic process, and the integral path is unified with the system trajectory, eliminating the power flow calculation at the steady-state point after the fault.

In summary, the system TEF expression based on the pre-fault steady-state point can be written as:

$$\begin{aligned} \hat{V} &= V_{KE} + \hat{V}_{PE} \\ &= V_{KE} + \hat{V}_{PE,m} + \hat{V}_{PE,w} + \hat{V}_{PE,l} + \hat{V}_{PE,b} \\ &= \sum_{i=1}^{n} \frac{1}{2} M_{gi} \Delta f_{gi}^2 - \sum_{i=1}^{n} \int_{t_0}^{t} (P_{mi} - P_{mi}^0) \Delta f_{gi} dt \\ &- \sum_{i=1}^{q} \int_{t_0}^{t} (P_{wi} - P_{wi}^0) \Delta f_{wi} dt \\ &+ \sum_{i=1}^{p} \int_{t_0}^{t} (P_{li} - P_{li}^0) \Delta f_{li} dt \\ &+ \sum_{b=1}^{k} \int_{t_0}^{t} (P_b - P_b^0) f_b \Delta f_b dt \end{aligned} \tag{9}$$

where $\hat{V}$ is the TEF of the system based on the pre-fault steady-state point, which differs from V by a constant C. $P_{mi,0}$, $P_{wi,0}$, and $P_{b,0}$ are the mechanical power, RES power, load power and line power in pre-fault steady state point. $\hat{V}_{PE,m}$, $\hat{V}_{PE,w}$, $\hat{V}_{PE,l}$ and $\hat{V}_{PE,b}$ are the total PE of generator, RES, load and line in the system based on the pre-fault steady-state point, respectively.

The TEF proposed in this paper is based on the pre-fault steady-state point, which allows the construction of the TEF based on the actual fault data trajectory. The energy model of each component is based on its port characteristics, which avoids complex internal model construction. Therefore, the TEF proposed in this paper can be directly based on system measurement data and does not require continuous modifications to the model.

2.3 Conversion principle of kinetic energy and potential energy

Combining (2) and (9) yields:

$$\frac{d\hat{V}}{dt} = 0 \Rightarrow \frac{dV_{KE}}{dt} = -\frac{d\hat{V}_{PE}}{dt} \tag{10}$$

It can be seen from (10) that the total energy of the system is constant, while in the transient process of the system, the PE and KE are converted equally along the post-fault trajectory. From the above analysis, integrating V_{KE} in any time period [t_a, t_b] results in:

$$V_{KE}|_{t_a}^{t_b} = \hat{V}_{PE}\Big|_{t_a}^{t_b} \tag{11}$$

Equation (11) reflects the relationship between the KE and PE of each component (generator, RES, load and line) in any time period [t_a, t_b] after the fault. Its meaning can be interpreted as being that after a large disturbance occurrence in the system, the rotor speed of the generator has a large deviation, and the KE released by the rotor into the system. The KE released by the rotor is characterized in each component in the form of PE. The greater the PE of an element, the more kinetic energy it absorbs, and the greater the impact of frequency deviation is. The connection between PE and system frequency is shown in Fig. 2. Therefore, the above analysis can quantitatively characterize the influence of each component in the system by the fault, and from the expression of PE, the disturbance degree of the component is related to the active power and frequency at the same time. This can provide a theoretical basis for the subsequent frequency control.

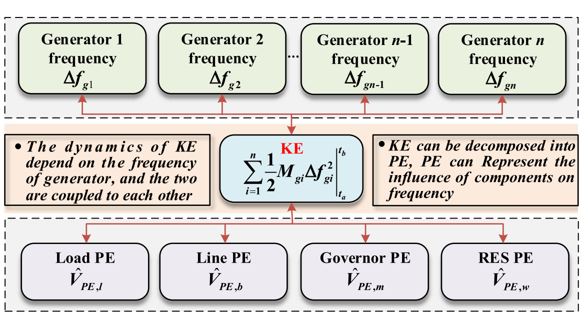

Fig. 2 The connection between PE and system frequency

3 Proposed hierarchical under frequency load shedding scheme

3.1 Unbalanced power calculation

1. *Calculation of Unbalanced Power under Loss of Synchronous Generation*: when a fault of loss of synchronous generator occurs in the system, the inertia of the system will change after the fault. If the system unbalanced power calculation is still performed according to the system inertia before the fault, the results will be incorrect. In order to accurately calculate the unbalanced power of the system, its calculation is based on the COI frequency of all synchronous generators in the system [10], as:

$$\Delta P_{LoG} = S_{post}M_{post}\frac{df_{coi}}{dt} \tag{12}$$

where ΔP_{LoG} is the system unbalanced power, $S_{post}M_{post}$ is the total inertia of the system after the fault, and f_{coi} is the COI frequency of the system.

Then, according to [10], the system unbalanced power expression under loss of synchronous generator can be obtained as:

$$\Delta P_{LoG} = \frac{S_{pre}M_{pre}}{1 - \frac{M_{loss}}{PF_{loss}}\frac{df_{coi}}{dt}}\frac{df_{coi}}{dt} \tag{13}$$

where PF_{loss} is the power factor constant of the lost synchronous generator, $S_{pre}M_{pre}$ is the total inertia of the system before the fault, and M_{loss} is the mechanical time constant of the lost synchronous generator.

However, the power factor constant and inertia of the lost generator after fault are unknown. Thus, if the change of the lost generator inertia is not considered in the unbalanced power calculation, the results may be too large, whereas if the lost inertia value considered is too large, the calculation results will be too small. Therefore, in order to calculate the unbalanced power accurately, this paper sets M_{loss} and PF_{loss} as the average inertia and average power factor of the lost synchronous generator.

2. *Load Characteristics Impact of Unbalanced Power Calculation*: after a fault occurs, the change of the system voltage and frequency will affect the active power of the load, which in turn affects the calculation of the unbalanced power. In the early stage after the fault occurrence, the voltage plays a leading role in the change of the active power of the load, while the frequency change is very small and can be ignored. Therefore, the voltage-dependent model of

the load can be considered in the unbalanced power calculation, as:

$$P_l = \sum_{i=1}^{p} P_{li0}[a_{pi}\tilde{U}_{li}^2 + b_{pi}\tilde{U}_{li} + c_{pi}] \tag{14}$$

where P_l is the total active power of the system load, P_{li0} is the active power of load i in the pre-fault steady-state, a_{pi}, b_{pi} and c_{pi} represent the proportions of constant impedance load, constant current load and constant power load, respectively. $\tilde{U}_{li}$ is the voltage per unit value of load i.

Then, the deviation of load active power can be expressed as:

$$\Delta P_l = \sum_{i=1}^{p} P_{li0}[a_{pi}\tilde{U}_{li}^2 + b_{pi}\tilde{U}_{li} + c_{pi} - 1] \tag{15}$$

In summary, the unbalanced power of the system can be expressed as the sum of the power deviations on the generation ΔP_{LoG} and demand ΔP_l, as:

$$\Delta P_{imb} = \Delta P_{LoG} + \Delta P_l \tag{16}$$

where ΔP_{imb} is the calculated system unbalanced power.

The unbalanced power estimation error is calculated as:

$$Evaluation\,Error\,rate = \left|\frac{\Delta P_{imb} - \Delta P_{true}}{\Delta P_{true}}\right| \times 100\% \tag{17}$$

where ΔP_{true} is the real unbalanced power in the system.

3.2 Load shedding amount allocation

From the analysis in Sect. 2, it can be seen that after a large disturbance occurrence in the system, if the PE of a load in a certain period of time is larger, the load is more affected by the fault. Therefore, the more the load is removed, the greater the impact on the KE of the system, and the more conducive to the recovery of the system frequency.

Therefore, for a multi-area inter-connected system, after the UFLS threshold is triggered by the system frequency, the shedding ratios of different loads can be expressed as:

$$\eta_j = \frac{\sum_{i=1}^{p_c} \hat{V}_{PE,li}\Big|_{t_1}^{t_{shed}}}{\hat{V}_{PE,l}\Big|_{t_1}^{t_{shed}}} \times 100\% \tag{18a}$$

$$\beta_{ji} = \frac{\hat{V}_{PE,li}\Big|_{t_1}^{t_{shed}}}{\sum_{i=1}^{p_c} \hat{V}_{PE,li}\Big|_{t_1}^{t_{shed}}} \times 100\% \tag{18b}$$

where t_1 and t_{shed} are the time when the imbalance power occurs and the UFLS relay actions, respectively. $\sum_{i=1}^{p_c} \hat{V}_{PE,li}$ is the total load PE in area j, p_c represents the number of loads with UFLS relays in area j, and $p_c \le p$. η_j and β_{ji} represent the proportion coefficients of LSA allocated to area j and load i in area j, respectively.

Therefore, the LSA of area j (δP_{lj}) and the LSA of load i in area j (δP_{lji}) can be expressed as:

$$\delta P_{lj} = \eta_j \times \Delta P_{shed} \tag{19a}$$

$$\delta P_{lji} = \beta_{ji} \times \delta P_{lj} \tag{19a}$$

where ΔP_{shed} represents the total amount of load power that needs to be shed by implementing the ULFS scheme.

3.3 Proposed hierarchical under frequency load shedding scheme

This paper adopts the hierarchical UFLS control strategy of " centralized real-time decision-making and decentralized real-time control", and makes full use of the UFLS relay and communication channel installed in the system. The control concept representation is shown in Fig. 3, and is realized by the centralized decision layer and decentralized control layer. The centralized decision layer includes the system decision center, which is mainly used to collect system information and transmit LS control objects and LS information to area control centers. The decentralized control layer is comprised of the area control center, which is mainly used to implement UFLS commands. These two layers are described in detail in the following paragraphs.

1. *Centralized decision layer*: It is mainly composed of the system decision center. Its main responsibilities include: receiving the key measurement information of the load and UFLS relay and identifying the system operational status; calculating the total controllable load of the system and the power imbalance

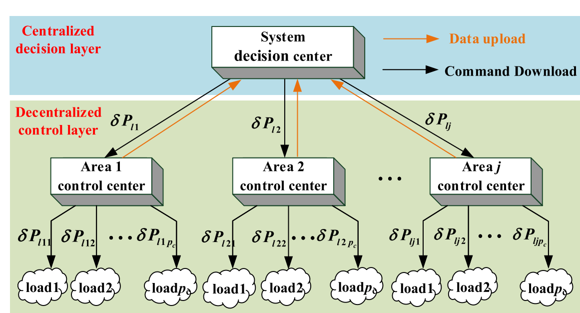

Fig. 3 The proposed hierarchical UFLS scheme control concept representation

in the case of system events; calculating the LS control object and LSA information after the event; and transmitting the LS command to each area control center.

2. *Decentralized control layer:* It is mainly composed of the area control center and the controllable load of each area. The area control center is responsible for communicating with the system decision center, uploading the key measurement information of load and UFLS relay state to the system decision center, receiving the LS command from the system decision center, and executing the LS operation.

The hierarchical UFLS scheme of the inter-connected system proposed in this paper needs to process the measurement data in the system decision center and send the LS command to the area control center, and then the area control center executes the LS operation. Therefore the time delay needs to be considered. Processing measurement data in the system control center usually requires consideration of the measurement factors and communication factors, totalling around 300 ms [17]. Similarly, the transmission of LS command from the system control center to the area control center and from the area control center to the UFLS relay typically requires consideration of the transmission times of 30 ms and 20 ms, respectively. In addition, considering that the LS circuit breaker tripping takes around 50 ms, there is a delay of approximately 400 ms between measurement data processing and LS circuit breaker action.

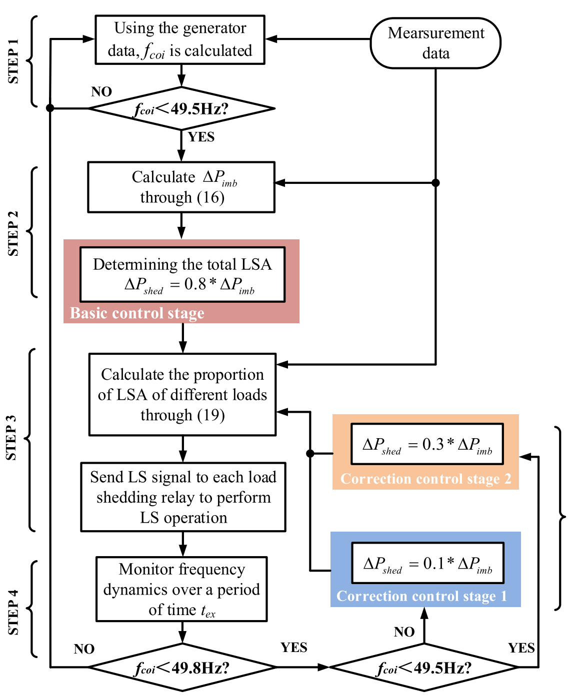

Fig. 4 Centralized decision-making process of the proposed hierarchical UFLS scheme

The centralized decision-making processes of the proposed hierarchical UFLS scheme are provided below, and the flow chart is shown in Fig. 4.

Step1: Using the generator data, f_{coi} is calculated. It is then compared with the UFLS relay frequency action threshold (e.g., 49.5 Hz) to decide whether to perform the UFLS operation. If $f_{coi} < 49.5$ Hz, the subsequent LS steps are performed.

Step2: Calculate the unbalanced power of the system using (16) and determine the total amount of load $\Delta P_{shed} = 0.8 * \Delta P_{imb}$ to be shed.

Step3: According to the collected data of loads equipped with UFLS relays, calculate the δP_{lji} of each load using (19), and send the LS signal to each UFLS relay to perform the LS operation.

Step4: Monitor whether the frequency exceeds the frequency safety limit of 49.8 Hz over a period of time t_{ex}. If $f_{coi} > 49.8$ Hz, returns to Step1.

Step5: If 49.5 Hz $< f_{coi} <$ 49.8 Hz, $\Delta P_{shed} = 0.1 * \Delta P_{imb}$, and If $f_{coi} < 49.5$ Hz, $\Delta P_{shed} = 0.3 * \Delta P_{imb}$. Returns to Step 3.

4 Simulation verification

This paper uses the modified New England 10-generator 39-bus system and a 197-bus real system in China in PSASP platform for simulation verification. In order to show the advantages of the proposed UFLS scheme, the following UFLS schemes are selected for comparison and verification:

1. The one-stage UFLS scheme, in which the LSA is evenly distributed among each load fitted with UFLS relays (Average Method);
2. The one-stage UFLS scheme, in which the LSA is distributed among each load fitted with UFLS relays according to the indicators proposed by [18];
3. The two-stage UFLS scheme proposed in [5];
4. The conventional four-stage UFLS scheme proposed in [9].

Here, the COI frequency and the actual LSA are used as the main performance indicators of the above UFLS scheme, including: the nadir frequency (f_{nadir}), post-fault steady-state frequency (f_{ss}), duration below 49.8 Hz frequency (t_d), and LSA (ΔP_{shed}).

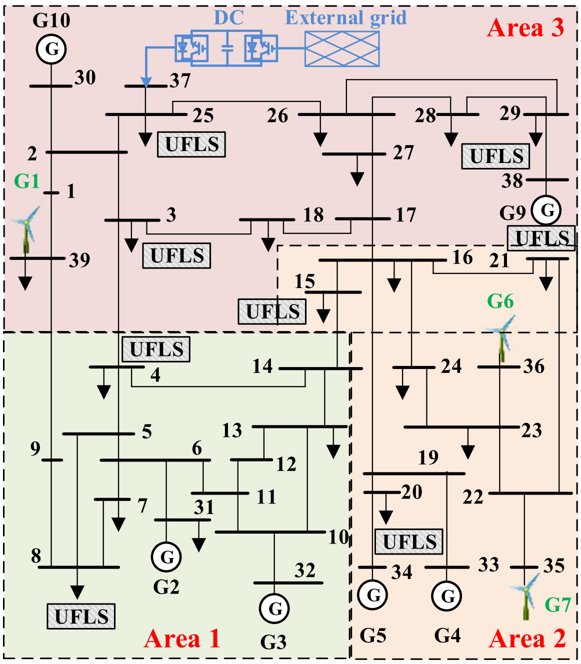

Fig. 5 Modified New England 10-generator 39-bus system

Table 1 The proportion of the PE and LSA of each area and load under loss of generator G3

Area	η_j (%)	Load	β_{li} (%)	δP_{li} (MW)
Area1	19	4	51	46.51
		8	49	44.69
Area2	52	15	0.64	1.61
		20	83.33	210.25
		21	16.03	40.44
Area3	29	3	38.43	54.46
		25	15.22	21.56
		29	46.35	65.68

4.1 Modified New England 10-generator 39-bus system

The proposed UFLS scheme is validated in the Modified New England 10-generator 39-bus system [24], as shown in Fig. 5. All the synchronous generators are equipped with governor models and all loads are constant impedance models in the simulation. The synchronous generators G1, G6 and G7 are replaced by a wind turbine with no virtual inertia control and fast frequency response. Synchronous generator G8 is replaced with a DC transmission to simulate external power transfer to the system. Considering the DC transmission, the system's RES penetration level reaches 45%. In actual systems, not all loads are fitted with UFLS relays. Therefore, in order to simulate the actual LS situation, not all loads in this study are fitted with UFLS relays, while loads randomly equipped with UFLS relays are identified in Fig. 5.

The preset parameter t_{ex} of the UFLS scheme proposed in this system is set to 30 s, while M_{loss} and PF_{loss} are set to 4 s and 0.85, respectively.

3. *Load shedding allocation*

Assuming that the failure results in the loss of synchronous generator G3 from the system, an unbalanced power of 650 MW appears in the system. The unbalanced power evaluated by (16) is 606.5 MW, indicating an evaluation error rate of 6.69%. According to the description in Sect. 3, the LSA of the proposed scheme is 485.2 MW.

Table 1 provides the proportions of PE and the LSA in each area. It can be seen from Table 1 that after G3 is lost, the PE of Area 2 is the largest, which indicates that the power and frequency of the overall load in this area are greatly deviated because of the influence of the fault. Likewise, Table 1 also presents the proportion of PE and the allocated LSA of loads equipped with UFLS relays in the area.

4. *Comparison of scheme effectiveness*

The proposed UFLS scheme in this paper performs LS operations according to the LSA allocated in Table 1, and its frequency response changes are shown in Fig. 6, which also shows the comparison of COI frequency changes under the proposed UFLS scheme and other different UFLS schemes. The frequency performance indicators of the different schemes are compared and presented in Table 2, and the LSA of the different schemes are shown in Fig. 7.

It can be seen from Fig. 6, Table 2 and Fig. 7 that, comparing the schemes composed of the proposed LSA allocation indicator, average allocation indicator, and the

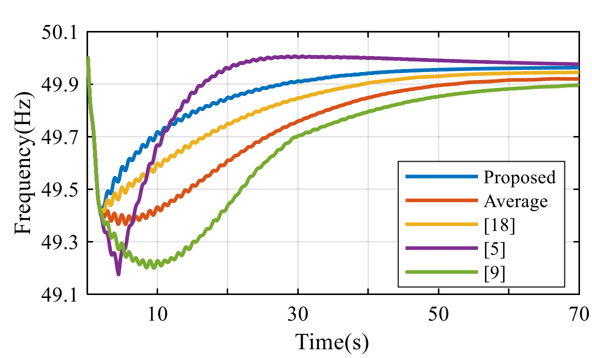

Fig. 6 The frequency response for loss of generator G3 under 45% RES penetration level

Table 2 Frequency performance indicators of 45% RES penetration levels under loss of generator G3

Method	f_{nadir} (Hz)	f_{ss} (Hz)	t_d (s)
Proposed	49.41	49.96	16.45
Average	49.37	49.92	33.98
[18]	49.41	49.94	24.01
[5]	49.17	49.98	13.20
[9]	49.19	49.90	40.80

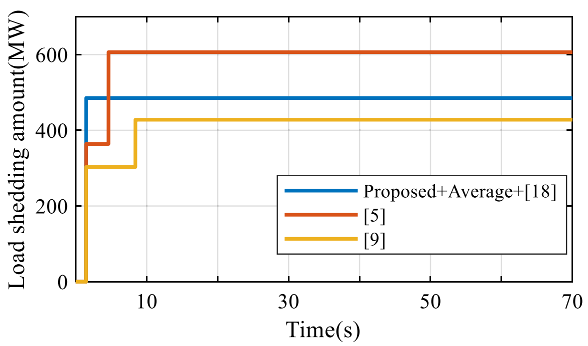

Fig. 7 The load shedding amount for loss of generator G3 under 45% RES penetration levels

indicator in [18], all three schemes have only one stage of UFLS and the same LSA, among which the f_{nadir}, f_{ss} and t_d of the proposed scheme are the best. This shows the advantages of using the proposed LSA allocation indicators in preventing frequency drop and facilitating frequency recovery. At the same time, the performance of UFLS with different LS stages is also discussed using the proposed LSA allocation indicators. The proposed scheme removes loads of 485.2 MW at 1.45 s. In scheme [5], LS is carried out at 1.45 s and 4.62 s, with 363.9 MW and 242.6 MW respectively. In scheme [9], the LS operation is performed at 1.45 s and 8.40 s, with 303 MW and 124.9 MW, respectively. The performance indicators of the three UFLS schemes in Table 2 and Fig. 7 are compared and ranked, as shown in Fig. 8a. As can be seen, the f_{nadir} indicator of the proposed scheme is ranked first, while the other three indicators are ranked second, indicating that the proposed scheme has no obvious shortcomings under the loss of generator G3, and is a relatively moderate scheme.

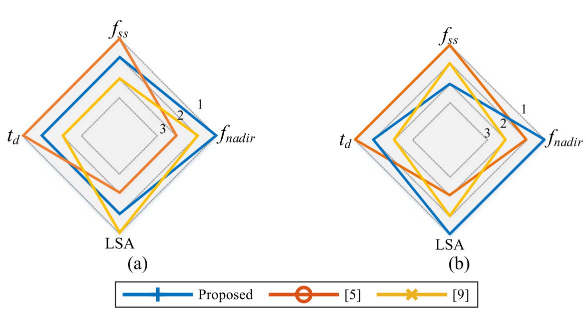

Fig. 8 Comparative ranking of performance indicators: **a** loss of generator G3, **b** DC bipole blocking

5. *Different renewable energy sources penetration levels*

In addition, Fig. 9 compares the performance indicators for UFLS schemes at different RES penetration levels. As can be seen from Fig. 9a, the increase of RES penetration levels leads to faster frequency change, which deteriorates the f_{nadir} of the five UFLS schemes, but the indicators of the proposed scheme are still the best. Figures 9b and c compare the performance of f_{ss} and t_d in different schemes. It can be seen that the performance indicators of the one-stage UFLS schemes (the proposed, average and [18]) deteriorate with the increase of RES penetration level. The multi-stage UFLS schemes ([5] and [9]) trigger more stages of LS with the increase of RES penetration level, as shown in Fig. 9d, making f_{ss} closer to 50 Hz and t_d shorter, but the LSA is larger.

Therefore for systems with high RES proportion levels (i.e., low inertia systems) unbalanced power disturbances can lead to faster rate of frequency drop and increase in the duration of frequency below 49.8 Hz. However, the impact on steady-state frequency and LS amount after faults is minimal.

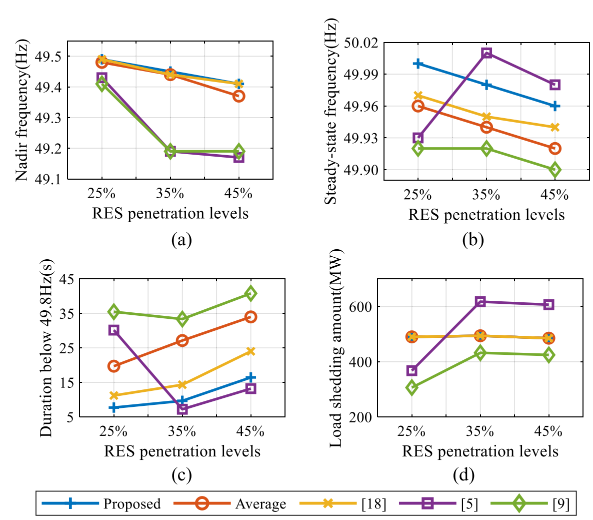

Fig. 9 Performance indicators of different RES penetration levels under loss of generator G3: **a** f_{nadir}, **b** f_{ss}, **c** t_d, **d** ΔP_{shed}

4.2 197-bus actual system in China

The 197-bus system is part of China's actual power grid, and is divided into two areas and contains 12 synchronous generators, 6 wind farms, 6 photovoltaic plants and one DC feed transmission channel, as shown in Fig. 10. The total power generated by the synchronous generators is 7180 MW, and the total power generated by the wind farms and photovoltaic plants is 1200 MW. In addition, the DC transmission power is 800 MW. As shown in Fig. 10, loads A8, A10, A14, A19, and A20 in area A, and loads B1, B2, B3, B5, and B6 in area B of the system are equipped with UFLS relays, which have higher priority for UFLS. The preset parameter t_{ex} of the UFLS scheme proposed in this system is 40 s, while M_{loss} and PF_{loss} are set to 7.7 s and 0.9, respectively.

The DC bipole blocking fault is simulated to verify the effectiveness of the proposed scheme in the actual system. This resulted in an 800 MW unbalanced power in the system, and the unbalanced power of the system evaluated using (16) is 725 MW, leading to an evaluation error rate of 9.38%. Since the loss of non-synchronous generation does not affect the moment of inertia of the system, using (16) to evaluate the unbalanced power of the system will cause the evaluation result to be lower than the actual value, leading to the increase of the evaluation error.

The method of obtaining LSA in each area and load is the same as that in Sect. 4. Because of space limitation, this section does not display the LSA.

The influence of wind speed variation on wind farm power is simulated. It is considered that the fluctuation power of the wind farm is connected to Bus1B-4, Bus1B-5 and Bus1B-6 during UFLS, while the power of the other RES remains unchanged. Then the total wind farm power fluctuates around 300 MW, and the specific changes are shown in Fig. 11. In this case, the frequency response changes and the performance indicators of the different schemes are shown in Fig. 11 and Table 3. It can be seen that, compared with other two different LSA allocation indicator schemes (average and [18]), the proposed scheme has better frequency recovery, and is least affected by wind power fluctuation in the frequency lifting process (10–50 s).

The performance indicators of the three UFLS schemes (the proposed, [5] and [9]) in Table 3 and Fig. 12 are compared and ranked, and the ranking results were shown in Fig. 8b. As can be seen from Fig. 8b, the t_d indicator of the proposed scheme is ranked last, but f_{nadir} and

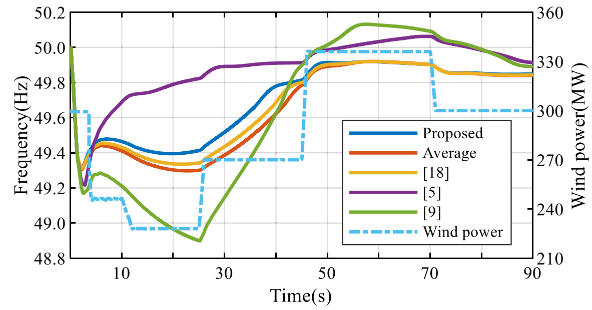

Fig. 11 The frequency response under DC bipole blocking fault

Table 3 Performance indicators under dc bipole blocking fault

Method	f_{nadir} (Hz)	f_{ss} (Hz)	t_d (s)
Proposed	49.31	49.85	42.01
Average	49.30	49.84	45.49
[18]	49.31	49.84	44.65
[5]	49.20	49.91	23.46
[9]	48.90	49.88	42.69

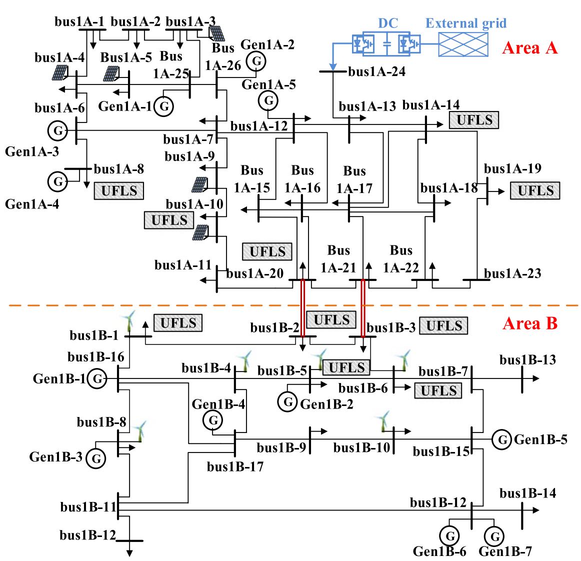

Fig. 10 The diagram of the 500 kV 197-bus system in China

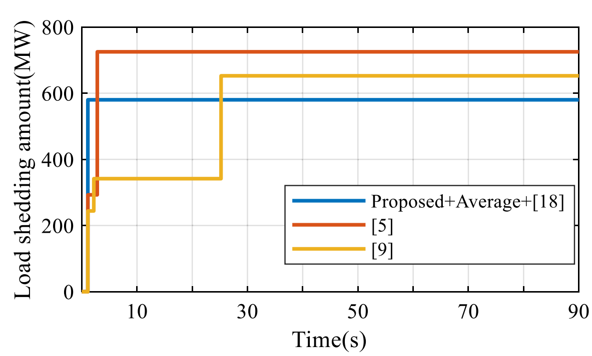

Fig. 12 The load shedding amount under DC bipole blocking fault

LSA indicators of the proposed scheme are ranked first, indicating that the proposed scheme can achieve the maximum f_{nadir} with the minimum LSA under DC bipole blocking.

It can be seen from both cases that the UFLS scheme proposed in this paper can effectively control the frequency indicator so that it is kept within a reasonable limit. In addition, in comparison with other UFLS schemes, the comprehensive analysis of the performance indicators confirms that the scheme proposed in this paper is appropriate.

5 Conclusion

In this paper, a hierarchical UFLS scheme of "centralized real-time decision-making and decentralized real-time control" based on measurement is proposed. In this scheme, a TEF is introduced to construct the system model. The TEF used in this paper is extended from [21] to be more suitable for system analysis under unbalanced power disturbance. According to the expression of the TEF, the dynamic process of the system is described as the process of mutual conversion of KE and PE. The PE of area and load is used for the calculation of the LSA allocation in the centralized decision layer, and the area and load with a high proportion of PE are allocated with more LSA, so that the KE in the system to be converted and absorbed is maximized to prevent the frequency from dropping quickly. At the same time, the one-stage UFLS process is implemented by the decentralized control center. The proposed scheme realizes coordinated control of load between regions and within regions, and improves the accuracy of UFLS as much as possible. The proposed hierarchical UFLS scheme is tested on the New England 10-generator 39-bus system and the 197-bus actual system in China. The results show that the proposed scheme can effectively control the system frequency within a reasonable range, and has good performance. Compared with other LSA allocation indicators, the proposed allocation indicators can achieve better frequency performance. In the high RES penetration scenario, compared with other multi-stage load shedding schemes, the proposed one-stage LS scheme can mitigate the impact of communication delay and obtain the maximum f_{nadir} with a small LSA.

The "centralized real-time decision-making and decentralized real-time control" framework used in this paper can achieve precise UFLS control. However, because of the transmission of information between different layers, control execution requires additional time. Therefore, the next research plan is to predict the time when the frequency reaches 49.5 Hz, so that the LS signal can be transmitted to the UFLS relay before the frequency threshold is reached. This can reduce the impact of time delay caused by data transmission on the UFLS performance.

Acknowledgements
The authors thank the National Key R&D Program of China "Response-driven intelligent enhanced analysis and control for bulk power system stability" [Grant Numbers 2021YFB2400800].

Author contributions
GC: Visualization, Investigation, Supervision methodology. SZ: Conceptualization, Software, Data curation, Writing-original draft. CL: Manuscript modification, Method correction. YZ, SG and ZC: Review & editing.

Funding
This work was supported in part by the National Key R&D Program of China "Response-driven intelligent enhanced analysis and control for bulk power system stability" under Grant 2021YFB2400800.

Availability of data and materials
The datasets used or analysed during the current study are available from the corresponding author on reasonable request.

Declarations

Competing interests
The authors declare that they have no known competing financial interests or personal relationships that could have appeared to influence the work reported in this paper.

Received: 1 March 2023 Accepted: 25 June 2023
Published online: 17 July 2023

References

1. Project Group Turkey. Report on blackout in Turkey on 31st March 2015-final version 1. 0[R]. ENTSO-E, 2015-09-21.
2. Zadeh, A. A., Sheikhi, A., & Sun, W. (2022). A novel probabilistic method for under frequency load shedding setting considering wind turbine response. *IEEE Transactions on Power Delivery, 37*(4), 2640–2649.
3. Potel, B., Debusschere, V., Cadoux, F., & Rudez, U. (2019). A real-time adjustment of conventional under-frequency load shedding thresholds. *IEEE Transactions on Power Delivery, 34*(6), 2272–2274.
4. Ma, J., Gu, Y., Shen, Y., Zhou, Y., Phadke, A. G., & Cheng, P. (2021). Stability analysis of power grid connected with direct-drive wind farm containing virtual inertia based on integrated dissipation energy model. *IEEE Transactions on Sustainable Energy, 12*(4), 2378–2392.
5. Kabir, Md. A., Hasib-Chowdhury, A., & Masood, N. A. (2020). A dynamic-adaptive load shedding methodology to improve frequency resilience of power systems. *International Journal of Electrical Power & Energy Systems, 122*, 106169.
6. Eremia, M., & Shahidehpour, M. (2013). *Handbook of electrical power system dynamics: modeling, stability, control*. Wiley.
7. Banijamali, S. S., & Amraee, T. (2019). Semi-adaptive setting of under frequency load shedding relays considering credible generation outage scenarios. *IEEE Transactions on Power Delivery, 34*(3), 1098–1108.
8. Terzija, V. V. (2006). Adaptive underfrequency load shedding based on the magnitude of the disturbance estimation. *IEEE Transactions on Power Systems, 21*(3), 1260–1266.
9. Rudez, U., & Mihalic, R. (2011). Monitoring the first frequency derivative to improve adaptive underfrequency load-shedding schemes. *IEEE Transactions on Power Systems, 26*(2), 839–846.
10. Sun, M., Liu, G., Popov, M., Terzija, V., & Azizi, S. (2021). Underfrequency load shedding using locally estimated RoCoF of the center of inertia. *IEEE Transactions on Power Systems, 36*(5), 4212–4222.
11. Laghari, J. A., Mokhlis, H., Karimi, M., Abu-Bakar, A. H., & Mohamad, H. (2015). A new under-frequency load shedding technique based on

combination of fixed and random priority of loads for smart grid applications. *IEEE Transactions on Power Systems, 30*(5), 2507–2515.
12. Jallad, J., et al. (2018). Improved UFLS with consideration of power deficit during shedding process and flexible load selection. *IET Renewable Power Generation, 12*(5), 565–575.
13. Prasetijo, D., & Lachs, W. R. (1994). A new load shedding scheme for limiting underfrequency. *IEEE Transactions on Power Systems, 9*(3), 1371–1378.
14. Sanaye-Pasand, M., Abedini, M., & Azizi, S. (2014). Adaptive load shedding scheme to preserve the power system stability following large disturbances. *IET Generation, Transmission & Distribution, 8*(12), 2124–2133.
15. Shekari, T., Aminifar, F., & Sanaye-Pasand, M. (2016). An analytical adaptive load shedding scheme against severe combinational disturbances. *IEEE Transactions on Power Systems, 31*(5), 4135–4143.
16. Mahari, A., & Seyedi, H. (2016). A wide area synchrophasor-based load shedding scheme to prevent voltage collapse. *International Journal of Electrical Power & Energy Systems, 78*, 248–257.
17. Chandra, A., & Pradhan, A. K. (2021). An adaptive underfrequency load shedding scheme in the presence of solar photovoltaic plants. *IEEE Systems Journal, 15*(1), 1235–1244.
18. Tang, J., Liu, J., Ponci, F., & Monti, A. (2013). Adaptive load shedding based on combined frequency and voltage stability assessment using synchrophasor measurements. *IEEE Transactions on Power Systems, 28*(2), 2035–2047.
19. Reddy, C. P., Chakrabarti, S., & Srivastava, S. C. (2014). A sensitivity-based method for under-frequency load-shedding. *IEEE Transactions on Power Systems, 29*(2), 984–985.
20. Odun-Ayo, T., & Crow, M. L. (2012). Structure-preserved power system transient stability using stochastic energy functions. *IEEE Transactions on Power Systems, 27*(3), 1450–1458.
21. Cai, G. W., Chan, K. W., Yuan, W. P., & Mu, G. (2007). Identification of the vulnerable transmission segment and cluster of critical machines using line transient potential energy. *International Journal of Electrical Power & Energy Systems, 29*(3), 199–207.
22. Elyasichamazkoti, F., Teimourzadeh, S., & Aminifar, F. (2022). Optimal distribution of power grid under-frequency load shedding with security considerations. *IEEE Transactions on Power Systems, 37*(5), 4110–4112.
23. Smon, I., Verbic, G., & Gubina, F. (2006). Local voltage-stability index using tellegen's theorem. *IEEE Transactions on Power Systems, 21*(3), 1267–1275.
24. Conte, F., Massucco, S., Paolone, M., et al. (2020). Frequency stability assessment of modern power systems: Models definition and parameters identification. *Sustainable Energy, Grids and Networks, 23*, 100384.